Composite Analysis of Large-Scale Environments Conducive to Western Pacific Polar/Subtropical Jet Superposition

ZACHARY J. HANDLOS AND JONATHAN E. MARTIN

University of Wisconsin–Madison, Madison, Wisconsin

(Manuscript received 4 January 2016, in final form 8 July 2016)

ABSTRACT

Although considerable research attention has been devoted to examination of the Northern Hemisphere polar and subtropical jet streams, relatively little has been directed toward understanding the circumstances that conspire to produce the relatively rare vertical superposition of these usually separate features. This study investigates the structure and evolution of large-scale environments associated with jet superposition events in the northwest Pacific. An objective identification scheme, using NCEP–NCAR Reanalysis 1 data, is employed to identify all jet superpositions in the western Pacific (30°–40°N, 135°–175°E) for boreal winters (DJF) between 1979/80 and 2009/10. The analysis reveals that environments conducive to western Pacific jet superposition share several large-scale features usually associated with East Asian winter monsoon (EAWM) northerly cold surges, including the presence of an enhanced Hadley cell–like circulation within the jet entrance region. It is further demonstrated that several EAWM indices are statistically significantly correlated with jet superposition frequency in the western Pacific. The life cycle of EAWM cold surges promotes interaction between tropical convection and internal jet dynamics. Low–potential vorticity (PV), high-θ_e air, appearing to be associated with anomalous convection in the western Pacific lower latitudes, is advected poleward toward the equatorward side of the jet in upper-tropospheric isentropic layers, resulting in anomalous anticyclonic wind shear that accelerates the jet. This, along with geostrophic cold air advection in the left jet entrance region that drives the polar tropopause downward through the jet core, promotes the development of the deep, vertical PV wall characteristic of superposed jets. A conceptual model synthesizing the results of this analysis is introduced.

1. Introduction

The Northern Hemisphere polar (PJ) and subtropical jet (STJ) streams are important elements in the large-scale circulation of the atmosphere and play a substantive role in the evolution of extratropical weather phenomena. In accord with thermal wind balance, the tropopause-level PJ generally resides in the upper troposphere within regions of strong lower- and mid-tropospheric baroclinicity (Reiter 1963). The STJ is confined to the upper troposphere and is associated with less substantial baroclinicity. Furthermore, the STJ is located on the poleward side of the Hadley cell circulation (Krishnamurti 1961), and angular momentum transport from equatorial latitudes poleward toward the subtropics is a strong driver of the STJ. Several decades of inquiry have been directed toward understanding the dynamics driving the maintenance of these jet streams as well as their effects on the development and propagation of weather systems (e.g., Namias and Clapp 1949; Loewe and Radok 1950a,b; Yeh 1950; Koetswaram 1953; Mohri 1953; Koetswaram and Parthasarathy 1954; Newton 1954; Sutcliffe and Bannon 1954; Defant and Taba 1957, hereafter DT57; Krishnamurti 1961; Riehl 1962; Reiter 1963; Palmén and Newton 1969; Keyser and Shapiro 1986; Shapiro and Keyser 1990).

The fact that both the PJ and STJ are associated with strong gradients in tropopause height follows from consideration of the quasigeostrophic potential vorticity (QGPV) equation, written as

$$q = \frac{1}{f_0}\nabla^2\phi + f + \frac{\partial}{\partial p}\left(\frac{f_0}{\sigma}\frac{\partial\phi}{\partial p}\right) = \Lambda(\phi) + f, \qquad (1)$$

where ϕ is geopotential, f is the Coriolis parameter, f_0 is a constant, σ is the static stability parameter, and

Corresponding author address: Jonathan E. Martin, University of Wisconsin–Madison, 1225 West Dayton St., Madison, WI 53706. E-mail: jemarti1@wisc.edu

DOI: 10.1175/JCLI-D-16-0044.1

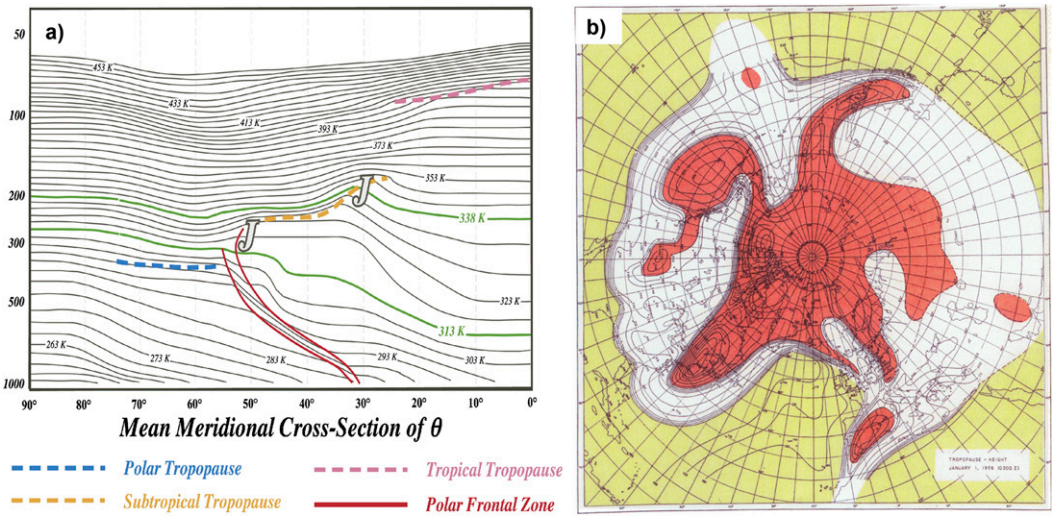

FIG. 1. (a) From Winters and Martin (2014), color-enhanced (from DT57) mean meridional cross section of isentropic (θ) surfaces (K; solid black lines) along with labeled jet stream locations (J symbols) and the tropical, subtropical, and polar tropopause steps [dashed contours; see legend at bottom of (a)] on 1 Jan 1956. The polar frontal zone is also labeled (solid red contour). (b) From DT57, tropopause height (hPa) over the Northern Hemisphere at 0300 UTC 1 Jan 1956. The yellow regions represent the tropical tropopause height, white regions represent the subtropical tropopause height, and red regions represent the polar tropopause height. The PJ (STJ) approximately resides along the strong concentrations in isolines bordering between the red and white (yellow and white) regions.

Λ is the second-order linear differential operator $\Lambda = (1/f_0)\nabla^2 + \partial/\partial p(f_0/\sigma)\partial/\partial p + (f_0/\sigma)\partial^2/\partial p^2$ (Cunningham and Keyser 2004). The across-flow gradient of QGPV $\partial q/\partial n$ is largest where the geostrophic wind V_g is largest since, from (1) and assuming f is constant:

$$\frac{\partial q}{\partial n} = \Lambda\left(\frac{\partial \phi}{\partial n}\right) = \Lambda(-f V_g). \tag{2}$$

DT57 were among the first to recognize this physical relationship. They identified three tropopause "steps" in the Northern Hemisphere: tropical, subtropical, and polar (Fig. 1). Both the PJ and STJ reside where the magnitude of the meridional gradient of tropopause height is large (Fig. 1b, recreated from DT57). The analysis of DT57 made it clear that there is often a separation in both altitude (Fig. 1a) and latitude (Fig. 1b) between the two jet species.

While relatively rare, there are instances in which the PJ and STJ become vertically superposed to form a single jet stream entity characterized by a deep tropopause wall that is bounded by two (rather than three) tropopause steps. An example of this "superposition" of the PJ and STJ can be seen in the North Atlantic Ocean in Fig. 1b as well as in the western Pacific region near Japan (DT57). It is clear that the subtropical tropopause step is essentially nonexistent within these two regions, and thus a single jet separates the tropical tropopause from the polar tropopause. An unusually large horizontal gradient in tropopause height and the presence of a deep, nearly vertical tropopause wall are the primary structural features associated with a superposed jet.

Very few prior studies have considered jet superposition events. Reiter (1961) and Reiter (1963) mention the possibility of PJ–STJ merger via vertical superposition of one jet stream on the other, with subsequent investigation of an example in Reiter and Whitney (1969). In that study, the authors investigate this phenomenon over the continental United States, stating that such merged jets do not seem to "behave" in the same manner as isolated PJ or STJ entities. A study by Mohri (1953) investigated PJ–STJ superposition in the western Pacific, representing the first such study (to our knowledge) that considered the occurrence of such an event in this region.

Recent work by Christenson (2013) and Winters and Martin (2014) has renewed investigation of vertical jet superposition events using an objective jet stream identification scheme (see section 2 for more details). Such events are defined as the vertical alignment of the PJ and STJ within a gridpoint column. Christenson (2013) constructs a climatology of such events, finding that, while superpositions are extremely rare in the Northern Hemisphere, the maximum frequency

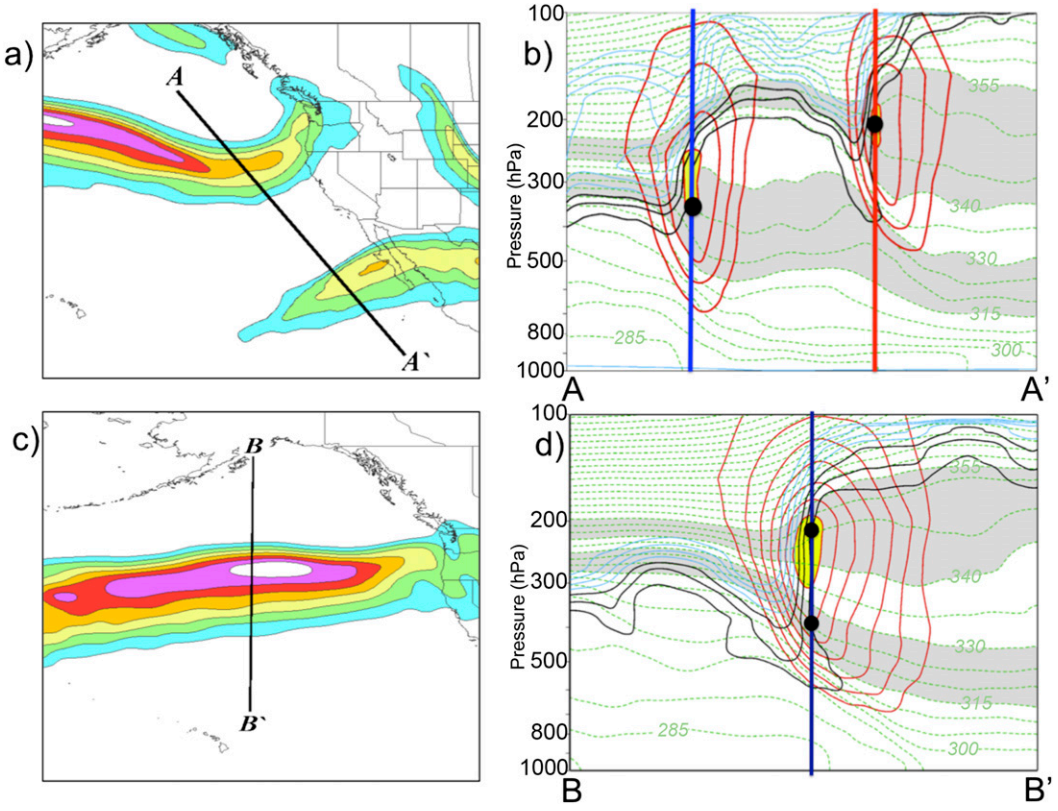

FIG. 2. From Winters and Martin (2014): (a) 300-hPa isotachs shaded every 10 m s^{-1} starting at 30 m s^{-1}, showing separate polar and subtropical jets near the U.S. West Coast at 0000 UTC 27 Apr 2010. (b) Cross section A–A′ through both the polar and subtropical jet cores from (a) with 1-, 2-, and 3-PVU surfaces contoured in black; 4-, 5-, 6-, 7-, 8-, and 9-PVU surfaces contoured in light blue; potential temperature contoured every 5 K in dashed green; and isotachs (red) every 10 m s^{-1} starting at 30 m s^{-1}. The PJ and STJ jet cores are shaded in yellow, and the 315–330- and 340–355-K isentropic layers (i.e., PJ and STJ isentropic layers, respectively) are shaded in gray. The blue (red) lines through a grid column with a black dot represent the identification of a polar (subtropical) jet. (c) As in (a), but for a vertical jet superposition event at 0000 UTC 24 Oct 2010. (d) As in (b), but for the cross section B–B′ in (c), with the PJ and STJ identifications (black dots) occurring within the same grid column, indicating a jet superposition.

of occurrence of superpositions occurs during boreal winter (i.e., December–February).

Winters and Martin (2014) show that a superposition event was an integral component of the 2010 Nashville, Tennessee, flood in the eastern United States. Other extreme weather events have been found to be associated with vertical jet superposition (Christenson 2013), and cursory reexamination of the synoptic environments identified in prior studies of significant weather events suggests some of them may have been associated with jet superposition (Hoskins and Berrisford 1988; Shapiro and Keyser 1990; Hakim et al. 1996; Bosart et al. 1996). Thus, understanding the physical processes involved in the development of jet superpositions as well as their role in significant weather-producing environments has both operational and phenomenological appeal.

To the best of our knowledge, no prior studies outside of Mohri (1953) have extensively investigated superposition events in the western Pacific. Since vertical jet superposition events are more common in the western Pacific during boreal winter than in any other region in the Northern Hemisphere (Christenson 2013), a goal of any study dedicated to examining this phenomenon is to determine why this region has more frequent superpositions. Therefore, the goal of the present study is twofold. First, we wish to determine what large-scale features are associated with western Pacific vertical jet superposition events during boreal winter. Second, we seek to identify the physical mechanisms that most commonly lead to jet superposition in this region.

The paper is organized as follows: In section 2, the dataset and methodology employed in constructing composite maps of western Pacific jet superpositions are described. Section 3 focuses on discussion of features that are associated with western Pacific vertical

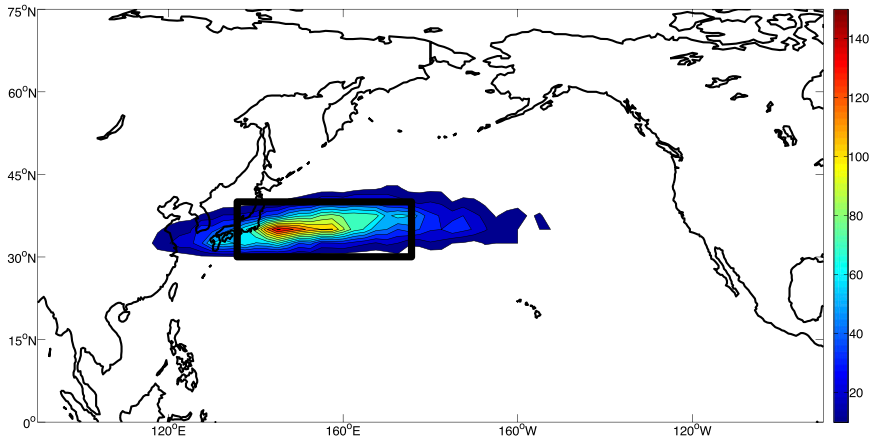

FIG. 3. Frequency of occurrence of vertical jet superposition events over the Pacific Ocean in the Northern Hemisphere during boreal winters 1979/80–2009/10. The black box region represents the region of interest in our study.

jet superpositions. In section 4, the evolution of those synoptic features and how their interactions lead to jet superposition is discussed. A summary and a discussion of the results are offered in section 5.

2. Data and methods

a. Data

The NCEP–NCAR Reanalysis 1 data (Kalnay et al. 1996) are employed for all variables and calculations utilized in this study. The data have a 2.5° horizontal grid spacing and 6-hourly temporal resolution. Data on both isobaric (unevenly spaced between 100 and 1000 hPa) and isentropic surfaces (interpolated every 5 K and examined in the 315–330- and 340–355-K layers)[1] are used. We focus on the months of December, January, and February (DJF) for all winters 1979/80–2009/10 (31 winters; leap days excluded).

b. Jet superposition identification scheme

We adopt the jet identification scheme used in Christenson (2013) and Winters and Martin (2014). The scheme is described with the aid of Fig. 2, which illustrates aspects of two different cases over the Pacific. Separate PJ and STJ features are clearly illustrated in the plan view in Fig. 2a. Figure 2b shows a vertical cross section through both jet cores. The polar jet core, located at approximately 300 hPa, is largely contained within the 315–330-K isentropic layer, while the subtropical jet core, located at approximately 200 hPa, occupies the 340–355-K layer (Fig. 2b). Both the subtropical and polar jet cores lie at the low–potential vorticity (PV) edge of the strong horizontal PV gradient that separates the upper troposphere from the lower stratosphere.

The scheme evaluates characteristics of the PV and wind speed distributions in each grid column. Within the 315–330-K (340–355-K) layer, whenever $|\nabla \mathrm{PV}|$ within the 1–3-PVU ($1\,\mathrm{PVU} = 10^{-6}\,\mathrm{K\,kg^{-1}\,m^2\,s^{-1}}$) channel exceeds or is equal to a threshold value[2] and the integrated wind speed in the 400–100-hPa layer $\geq 30\,\mathrm{m\,s^{-1}}$, we identify a polar (subtropical) jet in that grid column. The occurrence of both polar and subtropical jet characteristics in a single grid column identifies a jet superposition event at that time in that grid column. An example vertical cross section through an identified jet superposition[3] (Fig. 2c) is shown in Fig. 2d. Notice the steepness of the dynamic tropopause—a nearly vertical PV wall extends from ~550 to ~150 hPa—illustrating the leading structural characteristic of a jet superposition.

Figure 3 shows the frequency of occurrence of vertical jet superposition events over the North Pacific Ocean for boreal winters 1979/80–2009/10 using the objective identification scheme. It is clear that a maximum in such events resides over the western Pacific within the same region in which the near juxtaposition of the tropical and polar tropopauses in the DT57 analysis (Fig. 1) is observed. Based upon its being

[1] The 315–330- and 340–355-K layers were computed by averaging all levels between 315–330 and 340–355 K, respectively.

[2] The threshold value is 0.64×10^{-5} PVU $\mathrm{m^{-1}}$ for both the 315–330- and 340–355-K layers.

[3] Real-time identifications of the PJ, STJ, and jet superpositions using this identification scheme are available at http://marrella.aos.wisc.edu/JET/jet.html.

TABLE 1. Number of 6-hourly times where X number of vertical jet superposition IDs are found in the western Pacific region of interest (box in Fig. 3), where X is the value in the first column of this table.

X	No. of times with X IDs	Percent of 6-hourly times with X or more IDs
1	1451	13.0%
2	862	7.72%
3	532	4.77%
4	309	2.77%
5	184	1.65%
6	114	1.02%
7	66	0.591%
8	36	0.323%
9	22	0.197%
10	13	0.117%

centered on the maximum frequency of occurrence, we consider jet superposition events within the boxed region in Fig. 3.

c. Methodology

To investigate the physical mechanisms associated with the development of vertical jet superpositions in the western Pacific, a composite analysis of robust western Pacific superposition events is performed. The compositing procedure starts by identifying 6-hourly times in which superpositions occur in the boxed region in Fig. 3 (30°–40°N, 135°–175°E). A robust vertical superposition event is identified if the following criteria are satisfied: 1) at least seven vertical jet superposition identifications (IDs) occur simultaneously within the interest region; 2) during the 6-hourly time period before superposition, fewer IDs occur than at the time of superposition; and 3) during the 6-hourly time period after the time of superposition, no more than the number of IDs identified at the time of superposition occur within the box. The choice of a minimum ID threshold of 7 to define ''robust'' superposition events is motivated by the fact that such events are above the 99th percentile of all 6-hourly times we consider (Table 1).

After identifying all 6-hourly times meeting the above requirements (Table 2), meteorological quantities of interest are averaged over all cases identified in this analysis to construct composite maps of robust western Pacific superposition events. Specifically, we construct composite maps containing either anomalous or standardized anomalous quantities of interest as follows:

$$X_{\text{std.anom.}} = \frac{X_{\text{supj}} - X_{\text{climo}}}{X_{\text{stdclimo}}}, \tag{3}$$

TABLE 2. List of 44 robust western Pacific vertical jet superposition events identified using the methodology described in section 2c.

Robust event time and date	Robust event time and date
0000 UTC 7 Feb 1980	1200 UTC 14 Feb 1999
0600 UTC 29 Dec 1980	0000 UTC 23 Dec 1999
0600 UTC 11 Jan 1981	0600 UTC 31 Jan 2000
1200 UTC 29 Jan 1981	1200 UTC 16 Feb 2000
1800 UTC 14 Dec 1981	0000 UTC 17 Feb 2000
1800 UTC 15 Dec 1981	0600 UTC 11 Dec 2000
0600 UTC 4 Feb 1987	0000 UTC 4 Jan 2001
0000 UTC 10 Jan 1988	1200 UTC 4 Jan 2001
1200 UTC 23 Feb 1991	0000 UTC 15 Jan 2001
1800 UTC 24 Feb 1991	1200 UTC 15 Jan 2001
1200 UTC 25 Feb 1991	0000 UTC 16 Jan 2001
1800 UTC 24 Feb 1993	1800 UTC 19 Feb 2002
0000 UTC 25 Dec 1995	0000 UTC 21 Dec 2003
1800 UTC 25 Dec 1995	1800 UTC 26 Dec 2003
0000 UTC 1 Feb 1996	0600 UTC 7 Feb 2004
1200 UTC 2 Feb 1996	1800 UTC 27 Dec 2005
0000 UTC 1 Dec 1996	0000 UTC 10 Jan 2007
1200 UTC 1 Dec 1996	0000 UTC 15 Feb 2008
0000 UTC 2 Dec 1996	0000 UTC 16 Feb 2008
1200 UTC 9 Jan 1999	1800 UTC 16 Feb 2008
1200 UTC 12 Jan 1999	1200 UTC 8 Jan 2010
0000 UTC 13 Feb 1999	1200 UTC 15 Jan 2010

where $X_{\text{std.anom.}}$ is the standardized anomalous variable for a superposition event, X_{supj} is the variable measured at the point of interest at the time of the vertical jet superposition event, X_{climo} is the climatological value of the variable,[4] and X_{stdclimo} is the standard deviation of the 31-winter climatology of variable X.

In the next section, large-scale features associated with superposition events in the western Pacific are identified via the composite analysis. The evolution of these key features is then discussed in section 4.

3. Results

a. Key synoptic features associated with composite vertical jet superposition

Figure 4 shows various standardized anomalous quantities that characterize the environment associated with jet superpositions. The composite analysis reveals several key features that are also present during East Asian winter monsoon (EAWM) northerly cold surge events in the western Pacific during boreal winter. In

[4] The climatological value of X is the 31-winter average (i.e., 1979/80–2009/10) of variable X for that specific 6-hourly time in the reanalysis. For example, if a robust superposition occurred on 0000 UTC 14 February 2008, X_{climo} would be the 31-winter average of variable X at 0000 UTC 14 February.

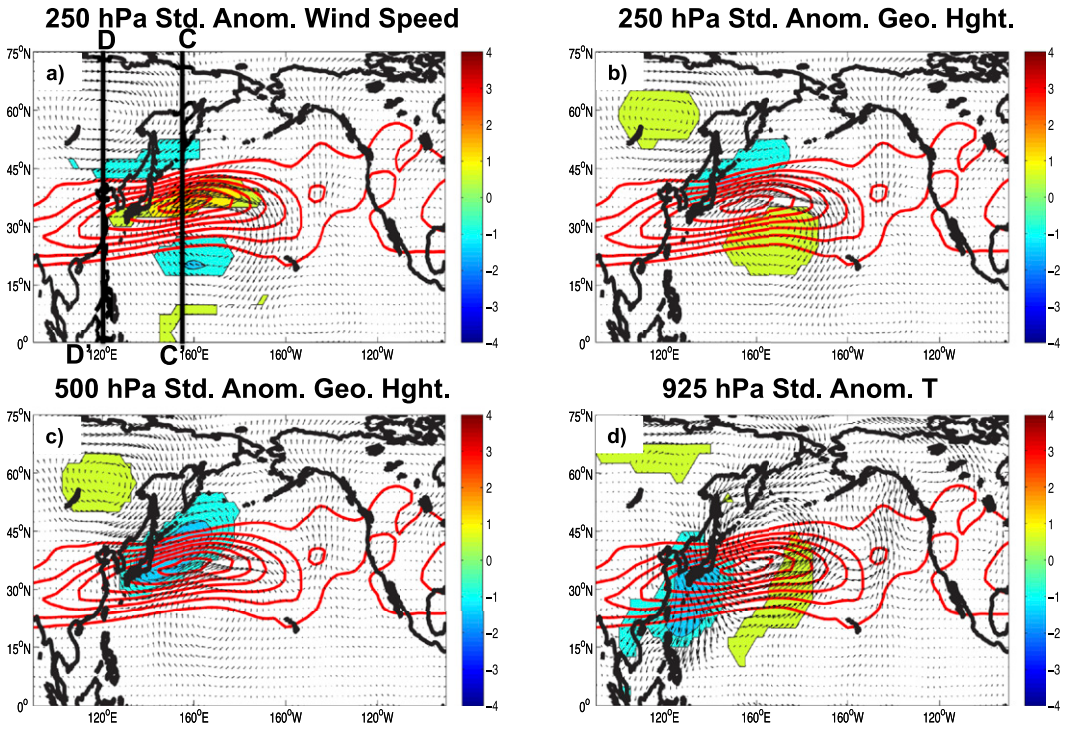

FIG. 4. Composite maps over the North Pacific Ocean: (a) $\overline{v}_{250,\text{std.anom.}}$ [fill pattern; yellow (blue) colors represent values $\geq 0.5\sigma$ ($\leq -0.5\sigma$) from climatology], (b) $\phi_{250,\text{std.anom.}}$ [same fill pattern conventions as (a)], (c) $\phi_{500,\text{std.anom.}}$ [same fill pattern conventions as (a)], and (d) $T_{925,\text{std.anom.}}$ [same fill pattern conventions as (a)]. On all maps, anomalous wind speeds at the level specified are plotted as vectors, and composite wind speed at 250 hPa is plotted as solid red contours every 10 m s^{-1} starting at 30 m s^{-1}. All maps are composite at the time of western Pacific vertical jet superposition. The cross-sectional lines C–C′ and D–D′ are relevant for Figs. 7 and 8, respectively.

Fig. 4a, $\overline{v}_{250,\text{std.anom.}}$ clearly shows a single jet stream entity in the western Pacific, with maximum wind speed in the jet core (located ~160°E) exceeding ≥ 90 m s^{-1}. Such speeds in the composite jet core exceed climatology by $>1.5\sigma$, while flanking anomalies north and south of the jet core are more than 1σ below climatology. This implies that the composite vertically superposed jet is not only faster but also narrower than climatology.

Figure 4b shows standardized anomalous geopotential height at 250 hPa ($\phi_{250,\text{std.anom}}$). An anomalous ϕ maximum (minimum) is present on the anticyclonic (cyclonic) shear side of the composite jet. There is also an anomalous ϕ maximum of $\geq 0.5\sigma$ in northern Russia. At 500 hPa (Fig. 4c), an anomalous trough feature resides just to the east of Japan, with $\phi_{500,\text{std.anom.}} < -1\sigma$. An anomalous anticyclonic feature in northern Russia exists at this level as well. An anomalous maximum in 500-hPa geopotential height also exists to the southeast of the trough.

Figure 4d shows 925-hPa standardized anomalous temperature ($T_{925,\text{std.anom.}}$). The combination of anomalous cold air and anomalous northerly wind over the East and South China Sea regions suggests that anomalous cold air advection is occurring there. Anomalously warm temperatures are present on the eastern side of the anomalous anticyclonic flow to the east of the "northerly cold surge" feature.

b. *East Asian winter monsoon cold surges and jet superpositions*

The EAWM is a boreal winter large-scale circulation phenomenon that is strongly a function of the strength of the Siberian–Mongolian surface high (SMH) pressure system (Chan and Li 2004). The SMH is, in turn, strongly a function of subsidence over the Tibetan Plateau and is a "cold" surface phenomenon, as it is tied to strong radiative cooling that persists over this region. Northerly cold surge events associated with the SMH occur on its eastern side, as the northerly winds associated with the SMH advect cold air as far south as the South China Sea region, leading to significant cold air outbreak events (Chin 1969; Morrice 1973; Chang et al. 1979; Chang and Lau 1980; Chan and Li 2004). Cold surges tied to the EAWM have been extensively investigated over the last several decades, as summarized (for example) in Boyle and Chen (1987) and Chan and Li (2004).

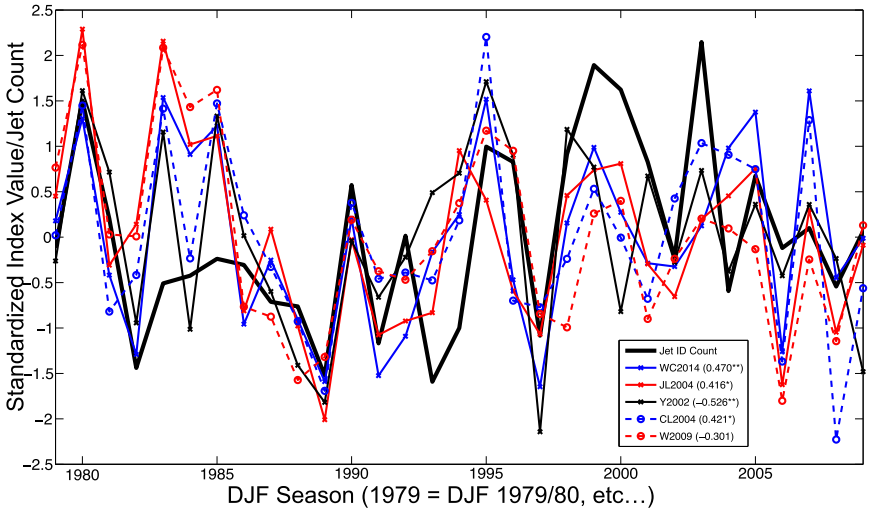

FIG. 5. Time series of cold season standardized jet superposition ID frequency in the western Pacific box region (thick black solid line) along with five standardized EAWM indices for winters 1979/80–2009/10. Note that, for the Yang et al. (2002) and Wang et al. (2009) time series plots, the time series were multiplied by −1 so that, for all indices shown, positive (negative) values imply strong (weak) EAWM winters. Also included are the correlation coefficients between each EAWM index and superposition ID frequency, where values with a single (double) asterisk are significant at the 95% (99%) level (note that we assume each winter season is independent of the others such that the number of degrees of freedom is $N - 2$, with $N = 31$).

A recent study by Wang and Chen (2014) utilizes a seasonal EAWM index based on normalized mean sea level pressure (MSLP) over Siberia, the North Pacific Ocean, and the Maritime Continent to determine large-scale features that are associated with strong and weak EAWM winters. In their Fig. 3, they showed that strong (weak) EAWM winters are associated with negative (positive) 500-hPa geopotential height anomalies east of Japan, stronger (weaker) 200-hPa zonal winds near the jet entrance region of the western Pacific jet, and anomalous northerly (southerly) wind at 850 hPa. The composite western Pacific jet superposition is also characterized by a strong wind speed along with a minimum in $\phi_{500\text{hPa}}$ over Japan and anomalous northerly winds in the lower troposphere. Other studies, such as Jhun and Lee (2004) and Wang and Chen (2010), using other EAWM indices, show that strong EAWM winters are characterized by the presence of similar large-scale features. Additionally, Lee et al. (2010) show that the subtropical Pacific jet is stronger (weaker) during strong (weak) EAWM winters.

The studies described above in conjunction with the results of our composite analysis suggest that jet superpositions may be a component of the large-scale circulation associated with EAWM northerly cold surge events. To further explore this possible relationship, the time series of total number of cold season superposition IDs in the box are compared to time series of several EAWM indices used in previous studies (Fig. 5). Four indices are selected from the list of 18 considered by Wang and Chen (2010). We also utilize the EAWM index from Wang and Chen (2014).

Figure 5 shows that the time series of the total number of western Pacific superposition IDs is similar to that of the various EAWM indices plotted. For the Jhun and Lee (2004) index (based on 300-hPa zonal wind speed), the number of superposition events increases with increased zonal wind speed. The region where the data were averaged is where the western Pacific jet in boreal winter frequently resides, implying a stronger (weaker) western Pacific jet magnitude during strong (weak) EAWM winters. Since a vertically superposed jet is associated with anomalously higher wind speed (Fig. 4a), the increase (decrease) in jet superposition IDs during strong (weak) EAWM winters is consistent with our composite results.

A negative correlation exists between ID counts and the Wang et al. (2009) EAWM index (based on using the first principal component extracted from a principal component analysis on $\phi_{500\text{hPa}}$), where negative (positive) index values indicate strong (weak) EAWM winters. The correlation implies more (less) jet superposition IDs with lower (higher) geopotential heights in the western Pacific region, where midtropospheric trough features develop and progress north of the location of the composite jet. Given that

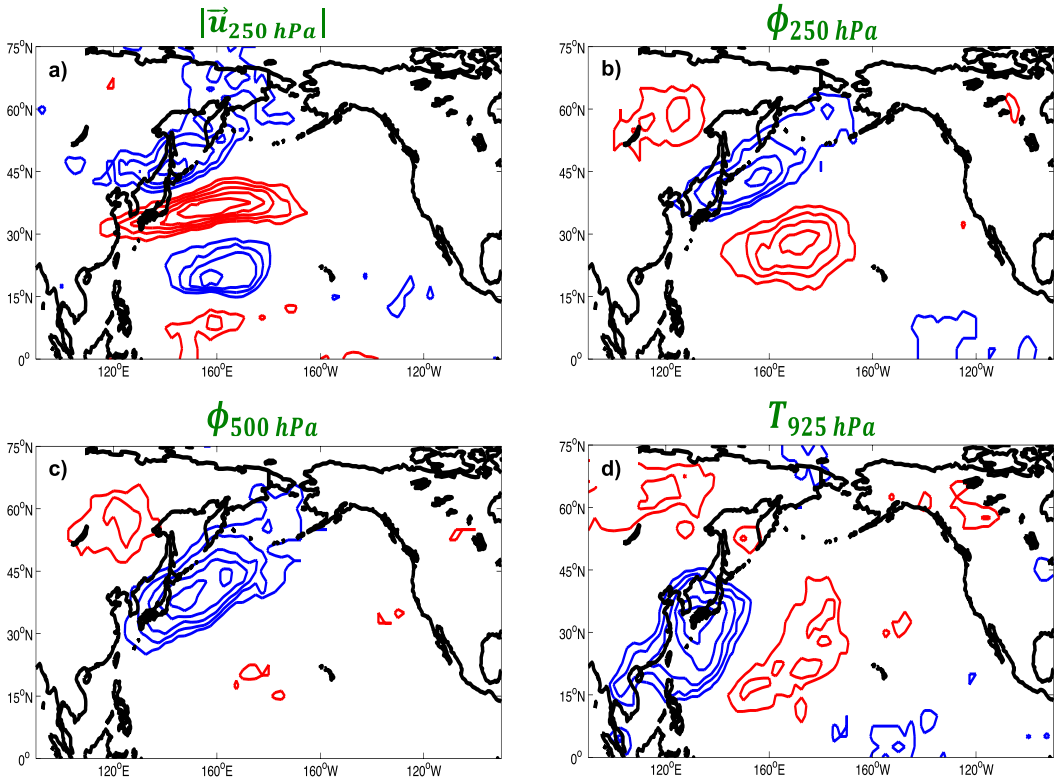

FIG. 6. Percent occurrence of each of the standardized variables in Fig. 4 for all 44 cases used in the composite. Red (blue) contours indicate regions where the variable of interest with standardized value $\geq 0.5\sigma$ ($\leq -0.5\sigma$) occurs in at least 50% of cases contoured every 10%. Variables in each panel match those of Fig. 4.

an anomalous trough at 500 hPa is observed north of the composite jet (Fig. 4c), the presence of anomalously negative $\phi_{500\text{hPa}}$ values in this region during seasons with more jet superposition events in the western Pacific (Fig. 5) is in line with our results.

There is a negative correlation between ID counts and the Yang et al. (2002) index (based on 850-hPa meridional wind), indicating that a stronger northerly wind is associated with a higher superposition ID frequency of occurrence and vice versa. Stronger northerly (southerly) winds imply a stronger (weaker) cold surge event pattern at 850 hPa and are thus associated with strong (weak) EAWM seasons. Given that a cold anomaly associated with composite anomalous northerly winds is observed in our composite analysis at 925 hPa (Fig. 4a) as well as at 850 hPa (not shown), the Fig. 4d result supports the correlation between jet superposition IDs and the Yang et al. (2002) index.

Finally, a positive correlation exists between the MSLP-based indices [i.e., the Chan and Li (2004) and Wang and Chen (2014) indices] and superposition ID counts. Strong (weak) EAWM winters have been shown to be associated with a stronger gradient in MSLP between the Siberian high and Aleutian low. Since the composite illustrates a strong MSLP gradient between the approximate location of the SMH and Aleutian low (not shown), the observation of higher (lower) jet superposition ID counts in the western Pacific with a higher (lower) index value is consistent with our composite results.

All correlations, except for the Wang et al. (2009) index, are statistically significant at least at the 95% confidence level. The v_{850} and normalized MSLP indices [i.e., Yang et al. (2002) and Wang and Chen (2014), respectively] are both significant at the 99% confidence level. In all cases, the sign of the correlation is such that more vertical jet superposition counts occur during stronger EAWM winters, and vice versa. Based on these simple correlations, we find a robust statistical relationship between the frequency of western Pacific superposition events and the strength of the EAWM.

c. *Frequency of occurrence of EAWM-like features from composite maps*

One of the disadvantages of performing a composite analysis is that large-scale synoptic features prominent within individual cases may be ‘‘smoothed out’’

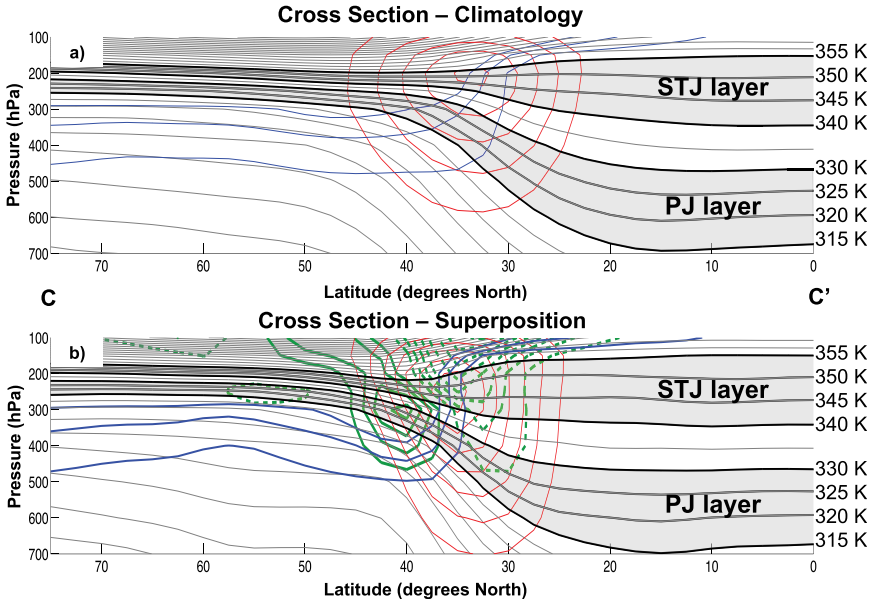

FIG. 7. (a) Climatological composite cross section taken along 155°E (C–C′ line from Fig. 4a) of wind speed (solid red contour; 10 m s^{-1} intervals starting at 30 m s^{-1}), isentropic surfaces (solid gray contour every 5 K starting at 280 K, with levels within 315–330- and 340–355-K layers in thicker black contour, labeled and shaded in light gray), and the 1–3-PVU channel in the upper troposphere (solid blue contour; PVU). (b) As in Fig. 7a, but for the composite superposition data, including anomalous Ertel PV [solid (dashed) green contour every 0.5 PVU starting at +0.5 (−0.5) PVU]. Note that the climatological composite cross section is computed by averaging together the climatological data for all 44 dates and times considered in this study, with the climatology for each date/time being the 31-yr average at that particular time.

within composite results. Similarly, large-magnitude features appearing in only a few cases (or even a single case) can exact an undue influence in the resulting composite. To minimize any associated misinterpretation of the composite results, the number of times at which, for each grid point, values of the standardized variables in Fig. 4 were greater than or less than 0.5σ from the mean was determined. That number was converted to a percentage of the 44 events in the composite. The results of this analysis are shown in Fig. 6.

Figure 6a shows that, within the core of the composite jet (Fig. 4a), ≥90% of the superposition events have $|\mathbf{u}_{250,\text{std.anom.}}| \geq 0.5\sigma$, with ≥70% of cases exhibiting $|\mathbf{u}_{250,\text{std.anom.}}| \leq -0.5\sigma$ in the flanking regions of reduced wind speed illustrated in Fig. 4a. Figure 6b shows that, for ≥50% of superposition cases, many of the grid points on the anticyclonic shear side of the composite jet are associated with $\phi_{250,\text{std.anom.}} \geq 0.5\sigma$. At the center of this feature, ≥80% of cases meet this criterion. The minimum in $\phi_{250,\text{std.anom.}}$ ($\leq -0.5\sigma$) near Japan is equally present in as many as 70%–80% of cases. Within the region where the composite trough feature at 500 hPa is present, $\phi_{500\text{hPa}} \leq -0.5\sigma$ for ≥80%–90% of superposition cases (Fig. 6c). This feature is present more consistently relative to the upper-tropospheric ridge and trough features indicated by $\phi_{250,\text{std.anom.}}$ in Fig. 6b. Interestingly, the anomalous geopotential height feature in the mid- to upper troposphere over northern Russia is only present within ≥50%–60% of the cases within a very localized region northeast (east) of Lake Baikal at 250 hPa (500 hPa).

As for the lower-tropospheric "northerly cold surge" feature, Fig. 6d shows that in the East and South China Sea regions, $T_{925\text{hPa}} \leq -0.5\sigma$ for ≥80%–90% of the superposition cases. Furthermore, the frequency of occurrence of $v_{925,\text{std.anom.}}$ in this region is $\leq -0.5\sigma$ for ≥50%–80% of cases (not shown). Thus, it is clear that the features highlighted in Fig. 4 are not only associated with strong EAWM winters and related cold surge events but also are quite common elements of the 44 cases that comprise the composite jet superposition (Fig. 6). Accordingly, we conclude that the majority of cases constituting the composite are associated with some sort of cold surge feature east of the coast of China.

d. Composite cross section results

The compositing methodology is next extended to the construction of composite cross sections that illuminate

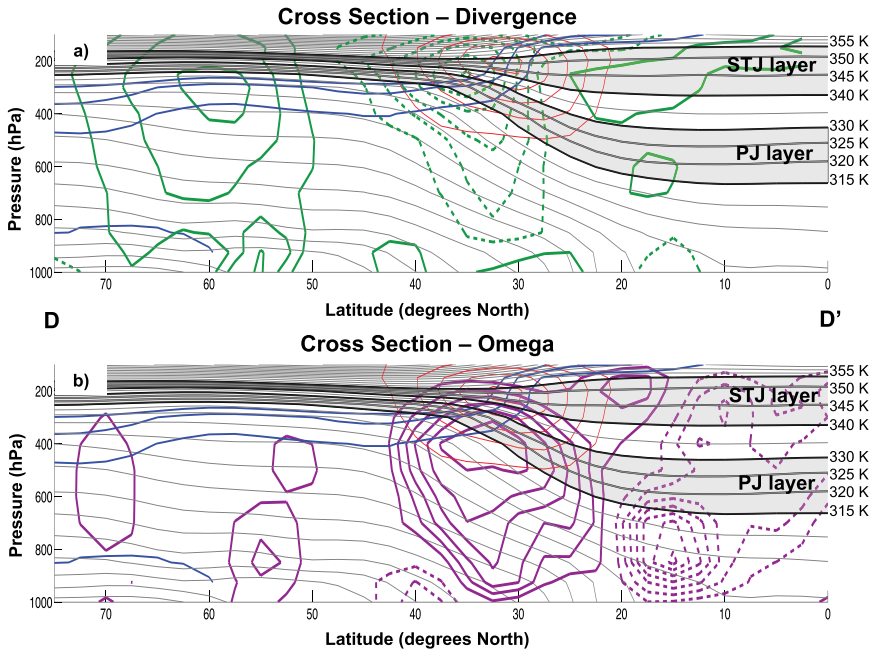

FIG. 8. Cross sections taken along 120°E (D–D′ line from Fig. 4a). All conventions are as in Fig. 7, (a) but the solid (dashed) green contour represents anomalous divergence (convergence) every $0.5 \times 10^{-6}\,s^{-1}$ starting at $+0.5$ $(-0.5) \times 10^{-6}\,s^{-1}$, and (b) the solid (dashed) purple contour represents anomalous downward (upward) vertical motion every $0.01\,Pa\,s^{-1}$ starting at $+0.01$ $(-0.01)\,Pa\,s^{-1}$.

the vertical structure associated with western Pacific jet composite superposition. Figure 7 shows both the climatological (Fig. 7a) and the superposition composite (Fig. 7b) vertical cross section along 155°E (line C–C′ in Fig. 4a) approximately through the composite jet core. It is clear that the composite superposition is characterized by a ''two-step'' tropopause, with a deep tropopause wall stretching from ~500 to 150 hPa and a jet core at ~250 hPa. The poleward tilt with height exhibited by the superposed jet (relative to the climatological jet) is associated with its much larger, and poleward tilted, horizontal temperature gradient, in accord with thermal wind balance.

Note that the PV ''wall'' is much stronger in magnitude (i.e., $|\nabla PV|$) and more vertically oriented in the composite superposition environment, as indicated by the region of negative (positive) anomalous PV located both equatorward (poleward) of and above (below) the composite jet core (Fig. 7b). The decrease (increase) in PV relative to climatology is associated with anomalously weak (strong) static stability on the equatorward (poleward) side of the composite jet within the STJ (PJ) isentropic layer (i.e., 340–355 K and 315–330 K, respectively). Finally, the jet core has a stronger wind speed maximum in the superposed composite than the climatology; this and the enhanced PV wall are features characteristic of a vertical jet superposition (Fig. 3).

Since vertical jet superposition events in the western Pacific appear to be associated with strong EAWM winters and cold surges, cross sections of the composite jet entrance region circulation (120°E) were considered in order to determine whether or not the jet entrance region circulation is enhanced (Fig. 8). The analysis is motivated by observational studies, such as Chang et al. (1979), Chang and Lau (1980), Wu and Chan (1997), and Yen and Chen (2002), that show an enhancement of the western Pacific jet as well as the ''local Hadley cell circulation'' spanning the Maritime Continent and east China regions during EAWM cold surge events. An enhanced jet entrance region circulation should be characterized by enhanced rising (sinking) motions equatorward (poleward) of the composite jet, with enhanced upper-tropospheric divergence (convergence), and vice versa at the surface.

Figure 8a shows anomalous divergence (convergence) in the upper troposphere equatorward (poleward) of the composite jet. Near the surface below each of these anomalies, the reverse occurs, with anomalous convergence (divergence) equatorward (near or poleward) of the jet. In fact, the anomalous jet entrance region circulation is displaced such that subsidence occurs beneath the jet core. Via mass continuity, anomalous upward (downward) vertical motion is present in the air column equatorward of (within) the jet core (Fig. 8b),

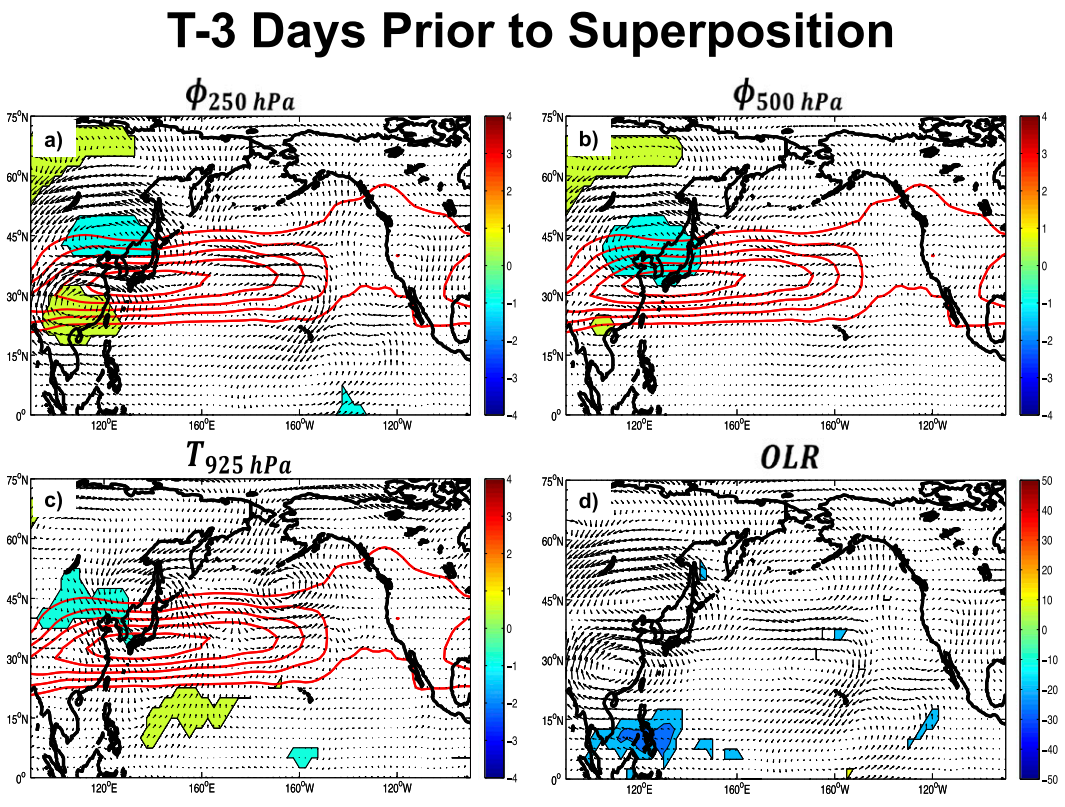

FIG. 9. Composite maps of (a) $\phi_{250,\text{std.anom.}}$, (b) $\phi_{500,\text{std.anom.}}$, (c) $T_{925,\text{std.anom.}}$, and (d) daily averaged anomalous interpolated OLR 3 days prior to composite western Pacific vertical jet superposition. Conventions are as in Fig. 4, but in the OLR plots the anomalous OLR values are contoured every 10 W m^{-2} starting at $\pm$10 W m^{-2}, and wind vectors represent 250-hPa anomalous wind (m s^{-1}).

representing an anomalous enhancement of the jet entrance region circulation.

While the analysis thus far reveals that the composite possesses the structural and dynamical characteristics of a superposed jet, nothing has been shown regarding the evolution of the environment that eventually produces such a jet. These issues are examined in the next section.

4. Lagged composite map analysis of western Pacific vertical jet superposition

a. Evolution of large-scale features associated with composite western Pacific superposition

To further investigate the physical mechanisms involved in the production of western Pacific jet superpositions, we construct composite maps at a series of times prior to the time of superposition (Figs. 9–11). At $T-3$ days, ($T=0$ is the day of jet superposition), the core of the western Pacific jet resides just south of Japan, with maximum 250-hPa wind speeds over 70 m s^{-1} (Fig. 9a). Unlike the composite shown in Fig. 4a, the anomalous flow on the anticyclonic shear side of the composite jet in Fig. 9a is near zero. However, an anomalous upper-tropospheric anticyclone with $\phi_{250,\text{std.anom.}} > 0.5\sigma$ is present near the right jet entrance region of the composite jet, while a minimum in $\phi_{250,\text{std.anom}}$ is present on the cyclonic shear side of the jet. There is also a region of $\phi_{250,\text{std.anom.}} > 0.5\sigma$ in northern Russia associated with anomalous anticyclonic flow.

At 500 hPa at this time (Fig. 9b), an anomalous troughlike feature is centered near the Korea peninsula with $\phi_{500,\text{std.anom.}} < -0.5\sigma$. A weak anomalous anticyclonic feature near the jet entrance region is also present, and the anomalous anticyclone observed in northern Russia at 250 hPa also exhibits a magnitude $>0.5\sigma$ at 500 hPa. At 925 hPa (Fig. 9c), anomalous cyclonic flow near the Korea peninsula and Japan suggests (along with Figs. 9a and 9b) the barotropic nature of the trough feature at this time. Anomalous cold air associated with strong anomalous northerly winds west of the Korea peninsula and weaker anomalous northerly winds over the South China Sea are also evident. Note that anomalous anticyclonic flow is also present in northern Russia, suggesting that this feature is

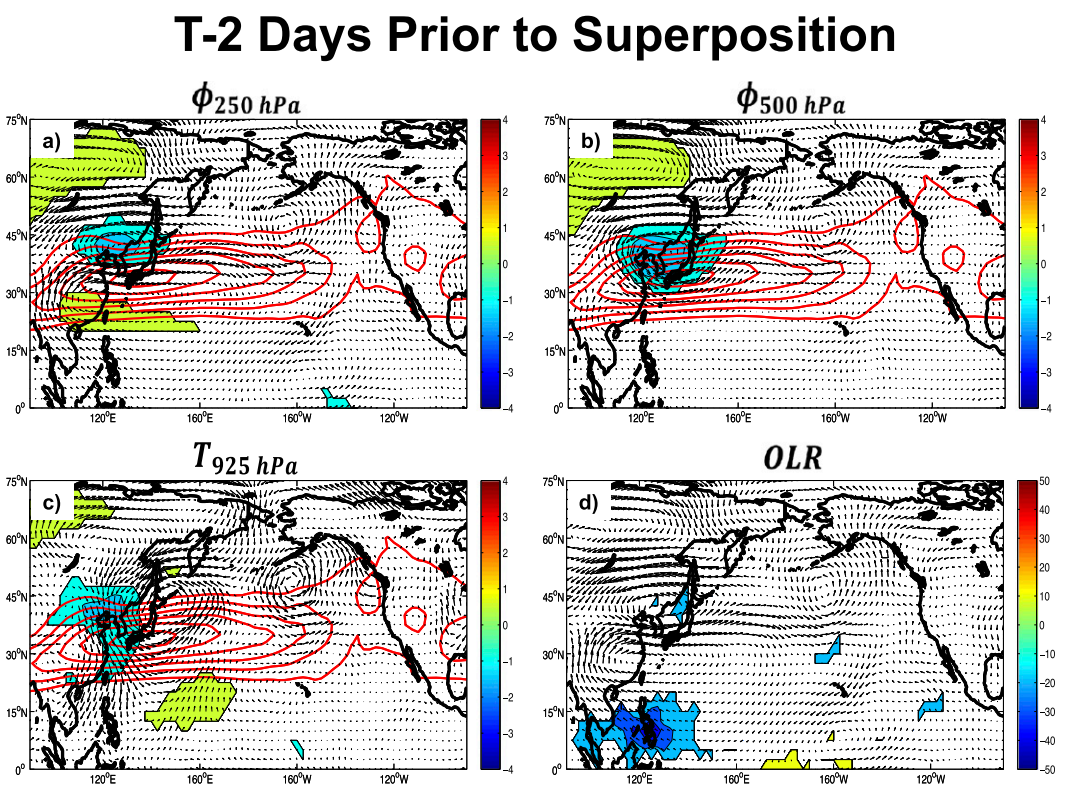

FIG. 10. As in Fig. 9, but the time prior to vertical jet superposition is 2 days rather than 3 days.

approximately barotropic in nature. Finally, Fig. 9d shows anomalous negative OLR values over the Maritime Continent, with the strongest values (in magnitude) confined to ~10°N, 130°E. To first order, negative OLR anomalies indicate regions of high cloud tops, likely resulting from composite anomalous convection.

By $T-2$ days, the magnitude of the western Pacific jet has intensified, with its core now centered east of southern Japan (Fig. 10a). The $\phi_{250,\text{std.anom.}}$ minimum along the cyclonic shear side of the composite jet has strengthened by this time, contributing to the enhancement of the composite jet speed. The composite trough at 500 hPa (Fig. 10b) has remained stationary while also intensifying. The anticyclonic flow southwest of the trough observed in Figs. 10a and 10b also remains stationary. The anomalous anticyclone in northern Russia in the mid- to upper troposphere moves eastward and strengthens.

The anomalous cold air and northerly winds associated with the composite cold surge over eastern China (Fig. 10c) have increased in magnitude while progressing southward at time $T-2$ days. Attendant with the advance of the cold air, the near-surface anomalous northerly winds at this time extend southward from the East China Sea toward the equator, leading to an increase in near-surface anomalous convergence (not shown). This convergence, in turn, contributes to forcing of anomalous upward vertical motion and the sustenance of anomalous convection in the lower latitudes (Fig. 10d).

Finally, by $T-1$ day, the composite jet is even stronger, with jet core wind speeds exceeding 90 m s^{-1} (Fig. 11a). A $\phi_{250,\text{std.anom}}$ maximum that is not discernible to the south of the jet core at $T-2$ days has grown in strength and areal coverage by this time. The composite $\phi_{250,\text{std.anom}}$ minimum near Japan continues its slow eastward propagation, while the $\phi_{250,\text{std.anom.}}$ maximum in northern Russia shifts slightly southward and weakens. The anomalous trough feature at 500 hPa (i.e., $\phi_{500,\text{std.anom.}}$ minimum) continues to move eastward as well, while the $\phi_{500,\text{std.anom.}}$ maximum in northern Russia evolves in a similar fashion as that observed at 250 hPa.

At 925 hPa, the composite cold surge feature and associated anomalous northerly winds continue to move equatorward as the anomalous cyclonic feature east of Japan continues to strengthen (Fig. 11c). The continued equatorward migration of cold air continues to fuel near-surface anomalous convergence, which maintains anomalous upward vertical motion and the associated convection in the lower latitudes (Fig. 11d). Note that this convection also spreads poleward at this time. The resulting enhancement of the rising branch of

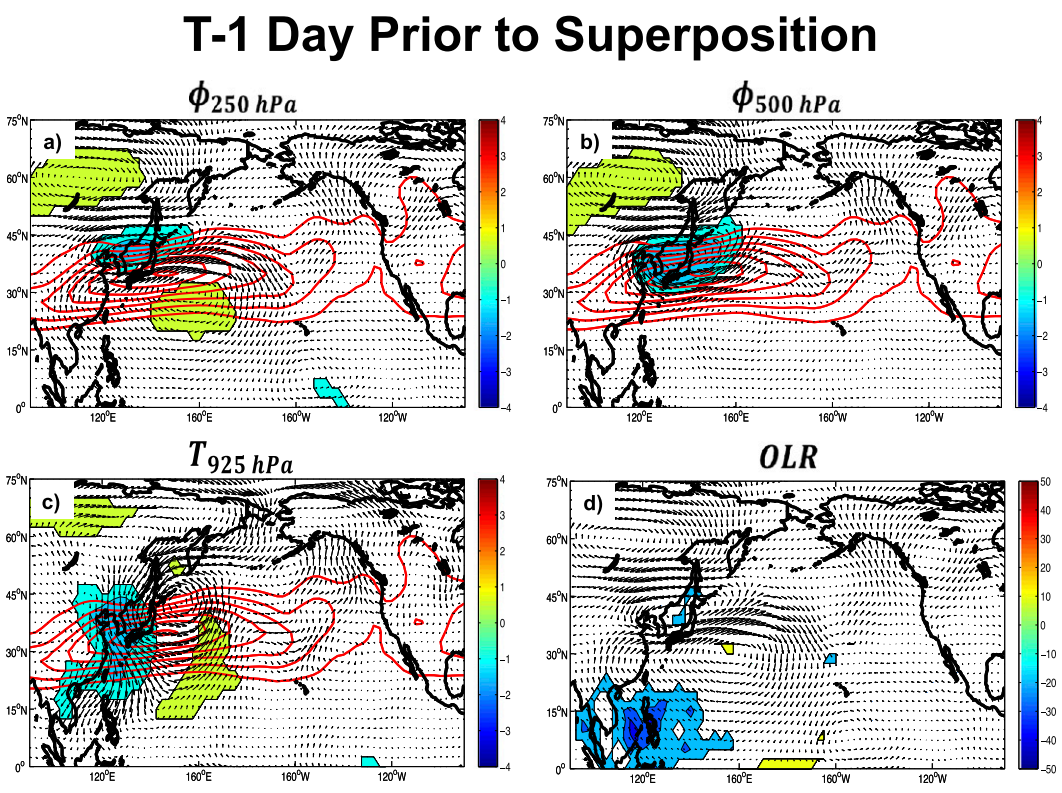

FIG. 11. As in Fig. 9, but the time prior to vertical jet superposition is 1 day rather than 3 days.

the local meridional overturning circulation plays a role in enhancing the entire composite jet entrance region circulation over the western Pacific, as observed in Fig. 8b.

b. *Evolution of deep, vertical PV wall associated with composite jet*

While Figs. 9–11 provide some insight regarding the evolution of the key synoptic features in the composites, they offer little explanation of how the deep PV wall structure associated with a negative (positive) PV anomaly on the anticyclonic (cyclonic) shear side of the composite jet develops. In this subsection, we investigate the physical mechanisms that reduce (increase) the magnitude of PV equatorward (poleward) of the jet.

First, to better understand the mechanisms responsible for the reduction in Ertel PV on the equatorward side of the composite superposed jet, we compute anomalous isentropic pressure depth within the 340–355-K isentropic layer, which houses the STJ. Figures 12 and 13 show plots of anomalous potential vorticity and anomalous pressure depth within the STJ isentropic layer, respectively, with the panels ordered from $T - 3$ days to composite superposition $T = 0$. Also plotted are the composite 1-, 2-, and 3-PVU contours as a guide to the tropopause location relative to the anomalous features of interest.

Figure 12 shows a negative PV anomaly that develops on the anticyclonic shear side of the composite jet core over the time period. Associated with this feature is a positive pressure depth anomaly (Fig. 13), which also propagates eastward and strengthens over time. The negative PV anomaly at $T - 3$ days (Fig. 12a) elongates and stretches eastward along the equatorward edge of the jet by $T - 2$ days (Fig. 12b). Subsequently, this feature becomes more intense and slightly more isotropic by $T - 1$ day (Fig. 12c)—a trend that continues through to the time of jet superposition (Fig. 12d). The singular negative PV anomaly becomes more negative throughout the 72-h period in association with an increase in magnitude of the positive pressure depth anomaly (Fig. 13).

The presence of the pressure depth anomaly equatorward of the composite jet has two effects on the composite jet core that play a significant role in inducing vertical jet superposition. First, increasing the pressure depth within the STJ layer on the anticyclonic shear side of the composite jet enhances the anomalous

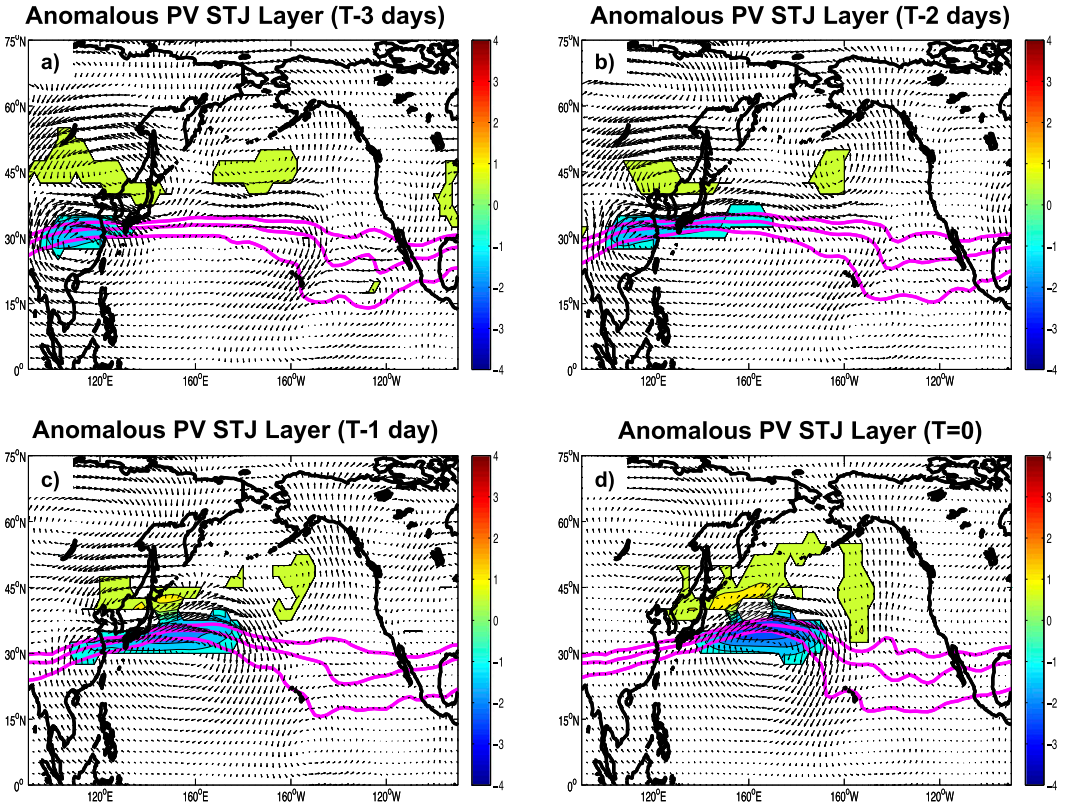

FIG. 12. Anomalous PV (PVU) within the STJ (340–355 K) isentropic layer (fill pattern) at (a) 3 days prior to composite superposition, (b) 2 days prior to composite superposition, (c) 1 day prior to composite superposition, and (d) at the time of composite superposition. The 1–3-PVU surfaces are contoured in solid purple. Anomalous winds within the STJ layer are shown as vectors.

anticyclonic flow in that layer in accord with the isentropic thermal wind equation:

$$\frac{\partial \mathbf{v}_g}{\partial \theta} = \frac{1}{f\rho\theta}\mathbf{k} \times \nabla p, \tag{4}$$

where ρ is the density of air. Thus, the expansion and intensification of the pressure depth anomaly on the equatorward side of the jet seen in Fig. 13 is associated with an anomalous anticyclonic vertical geostrophic wind shear that contributes to the anomalous wind speed in the jet core.

Second, the coincidence of the negative PV anomalies in Fig. 12 with the positive perturbation pressure depths in Fig. 13 may be a function of the fact that the air that fills the STJ layer originates in the tropical/subtropical boundary layer, where θ_e is large and PV is small. To illustrate this connection, we adopt a Lagrangian perspective and investigate air parcel back trajectories generated using the Air Resources Laboratory (ARL) Hybrid Single-Particle Lagrangian Integrated Trajectory (HYSPLIT) model (Draxler and Hess 1997, 1998; Draxler 1999; Draxler and Rolph 2015; Rolph 2015). Specifically, we compute back trajectories from the location of the center of the positive pressure depth anomaly maximum at the time of composite superposition (Fig. 13d) for all robust superposition cases we consider.

The results of this analysis are shown in Fig. 14, which shows single air parcel back trajectories in plan view for each case calculated starting at 32.5°N, 160°E. Parcel trajectories starting at altitudes of 10 and 12 km are shown in blue and red, respectively. Figure 14b shows the potential temperature θ associated with each trajectory, and Fig. 14c the altitude associated with each parcel over a 120-h period. It is clear that the majority of the air parcels came from lower latitudes within the vicinity of the negative anomalous OLR observed in Figs. 9d, 10d, and 11d, with a few back trajectories extending westward past the prime meridian. Nearly all of the parcels remain within the mid- to upper troposphere between $T - 5$ days and $T = 0$ days (Fig. 14c), tracing the anomalous anticyclonic flow observed in this region (Figs. 4a,b). The θ values associated with these trajectories (Fig. 14b) demonstrate that the majority of air parcels remain within

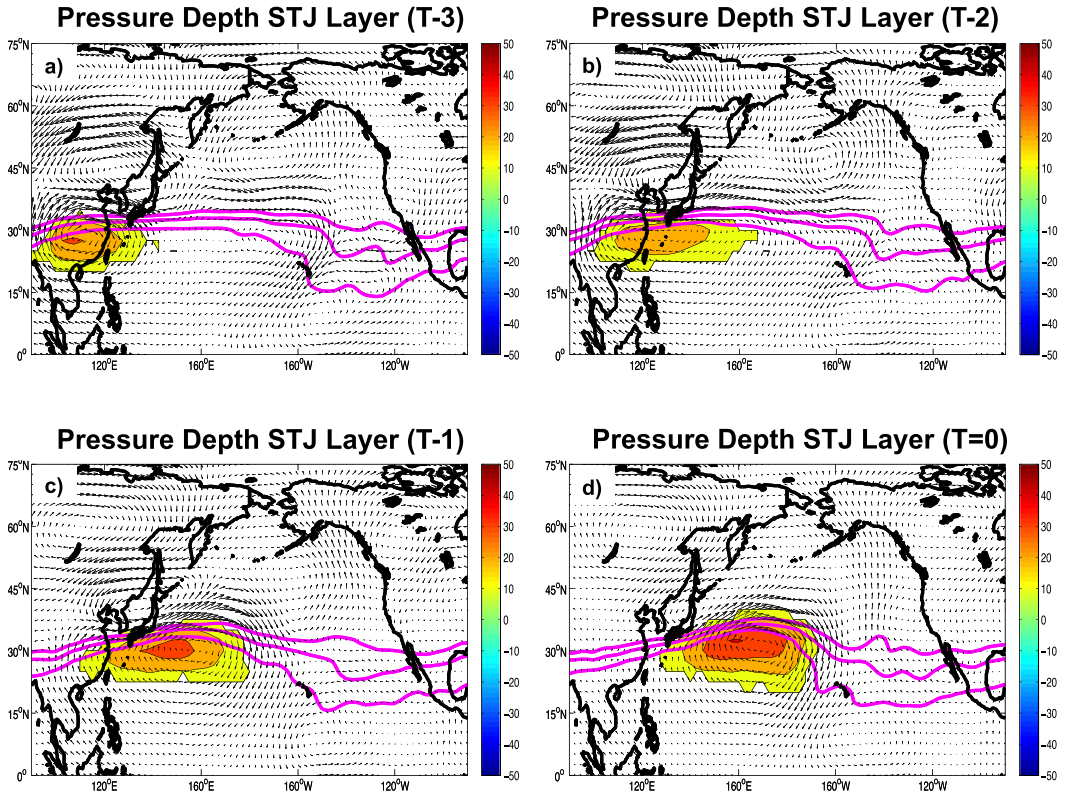

FIG. 13. Composite anomalous pressure depth within the STJ (340–355 K) isentropic layer (fill pattern) at (a) 3 days prior to composite superposition, (b) 2 days prior to composite superposition, (c) 1 day prior to composite superposition, and (d) at the time of composite superposition. Note that $dp = p_{340\mathrm{K}} - p_{355\mathrm{K}}$ for the 340–355-K isentropic layer. The 1–3-PVU surfaces are contoured in solid purple. Anomalous winds within the STJ layer are shown as vectors.

the STJ layer throughout the period. Several of these air parcels increased their θ value diabatically over time and ultimately ended up within the STJ layer (Figs. 14b,c).

The location of many of these parcels over the anomalous negative OLR suggests that upper-tropospheric exhaust from convection in the South China Sea may play a role in systematically exporting tropical boundary layer air upward. The anomalous anticyclonic flow present equatorward of the jet then transports this high-θ_e, low-PV air poleward and eastward into the STJ layer on the anticyclonic shear side of the western Pacific jet. This process results not only in an enhancement of the jet core wind speed (via anomalous geostrophic vertical shear associated with the deposition of mass on the south side of the jet), but also accounts for the importation of the negative PV anomaly on that side of the jet that contributes to steepening the PV wall characteristic of a superposed jet.

On the poleward side of the jet, a positive PV anomaly within the PJ isentropic layer (associated with the upper-tropospheric anomalous trough) propagates eastward over the 72-h period (Fig. 15). At the time of superposition, the positive PV anomaly resides on the poleward side of the composite jet to the northwest of the composite negative PV anomaly within the STJ layer. This feature is responsible for the positive PV anomaly observed in Fig. 7b and therefore also plays a role in strengthening the PV wall associated with the superposed jet.

Recall from Fig. 8b that the jet entrance region circulation associated with the composite superposed jet is both anomalously strong and shifted equatorward. This equatorward shift places the region of anomalous subsidence directly beneath the composite jet core. Such a distribution promotes downward extrusion of stratospheric air into the upper troposphere and is dynamically related to the presence of geostrophic cold air advection in cyclonic shear (e.g., Eliassen 1962; Shapiro 1982; Keyser and Pecnick 1985; Martin 2014).

Figure 16 shows composite geostrophic temperature advection and vertical motion at 300 hPa (the isobaric

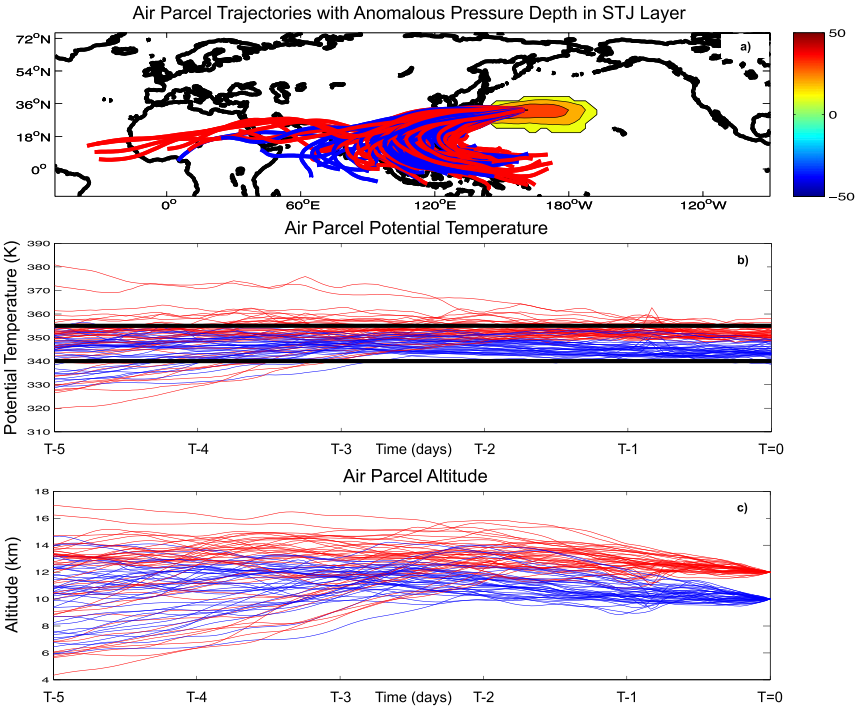

FIG. 14. (a) As in Fig. 13d, but included are ARL HYSPLIT 120-h back trajectories for air parcels, where the trajectories begin at the center of the anomalous pressure depth feature within the STJ isentropic layer (32.5°N, 160°E). Trajectories colored in blue (red) represent parcels with back trajectories starting at 10 km (12 km). (b) Time series of θ (K) associated with each parcel back trajectory shown in (a). Color conventions for the time series are the same as that of the trajectories from (a). The STJ isentropic layer lies between the solid black lines (340–355 K). (c) Time series of altitude (km) associated with each parcel back trajectory shown in (a). The color conventions are as in (b).

level at which the PJ approximately resides) at times $T - 3$, $T - 2$, and $T - 1$ prior to composite jet superposition (Figs. 16a, 16b, and 16c, respectively) as well as at time $T = 0$ (Fig. 16d). It is clear that geostrophic cold air advection is present on the cyclonic shear side of the composite jet entrance region and that the regions of composite cold air advection are associated with composite subsidence. This subsidence, acting throughout the entire 72-h period prior to superposition, drags high-PV air downward from the lower stratosphere on the poleward side of the jet along the sloping isentropic surfaces within the region of maximum anomalous subsidence shown in Fig. 8b. This process plays a central role in creating the anomalous positive PV feature found on the poleward side of the composite superposed jet (Fig. 7b). Thus, the juxtaposition of opposing PV anomalies across the composite superposed jet (portrayed in Fig. 7b) is a result of internal jet dynamics lowering the polar tropopause on its cyclonic shear side, acting in concert with a raising of the subtropical tropopause on its anticyclonic shear side through transport of low-PV, high-θ_e air into the STJ layer.

5. Discussion and conclusions

In this paper, an investigation of the structure and evolution of the large-scale features most commonly associated with wintertime vertical jet superposition events in the western Pacific has been presented. The study focused on composite analysis of 44 particularly robust superposition events observed over 31 winters using the NCEP–NCAR Reanalysis 1 dataset.

The analysis reveals that the most robust synoptic features associated with western Pacific jet superposition events are 1) a single, strong and latitudinally narrow composite western Pacific jet stream with a wind speed maximum of $\geq 90\,\mathrm{m\,s^{-1}}$; 2) a positive/negative couplet of $\phi_{250,\mathrm{std.anom.}}$ anomaly straddling the composite western Pacific jet; 3) an anomalous trough ($\phi_{500,\mathrm{std.anom.}}$ minimum) on the cyclonic shear side of the composite jet; and 4) a negative $T_{925,\mathrm{std.anom.}}$ feature that resembles a ''cold surge'' type of event that occurs during strong

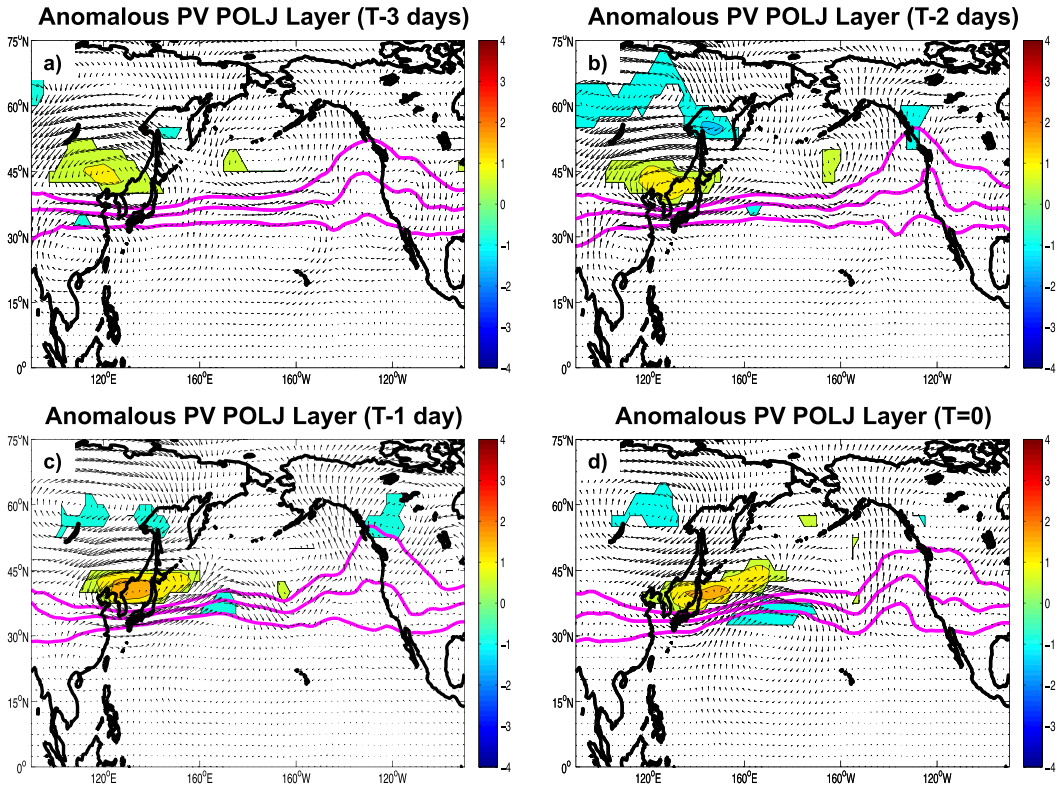

FIG. 15. Anomalous PV (PVU) within the PJ (315–330 K) isentropic layer (fill pattern) at (a) 3 days prior to composite superposition, (b) 2 days prior to composite superposition, (c) 1 day prior to composite superposition, and (d) at the time of composite superposition. The 1–3-PVU surfaces are contoured in solid purple. Anomalous winds within the PJ layer are shown as vectors.

EAWM winters (Fig. 4). All of these features are shown to occur within the majority of the superposition events selected for the analysis (Fig. 6).

The simultaneous presence of a strong jet along with midtropospheric trough and cold surge anomalies is also a characteristic feature of EAWM cold surge events, suggesting that western Pacific jet superposition events may be preferentially tied to the cold surges of strong EAWM winters. Statistical support for this suggestion arises from the fact that several EAWM indices are significantly correlated with the number of jet superposition IDs that occur in the western Pacific analysis region (Fig. 5). Future work will include further exploration of this suggested relationship.

Cross sections through the composite jet core (Fig. 7) show a two-step tropopause and a deep PV wall through the jet; both the stronger winds and deeper PV wall relative to climatology are features characteristic of western Pacific jet superpositions (Fig. 3d). Also, negative (positive) anomalous Ertel PV equatorward (poleward) of the jet core is present (Fig. 7b), associated with weak (strong) static stability within the STJ isentropic layer (Fig. 7b). The jet entrance region circulation associated with the composite superposed jet is also stronger relative to climatology (Fig. 8) and is shifted equatorward such that subsidence occurs beneath the jet core in its entrance region.

To better understand the evolution of key synoptic features that lead to robust western Pacific jet superposition, composite maps at times 1–3 days prior to composite jet superposition were constructed. The relationship between these key features and their respective evolutions is summarized in a conceptual model illustrated in Fig. 17. A near-surface cold air anomaly is located in northeastern China 3 days prior to composite jet superposition (Fig. 17a). Anomalous convection in the tropical western Pacific (cloud symbols in Fig. 17a) is also present. As the cold pool moves equatorward over time, the associated anomalous northerly winds (purple arrows in Fig. 17) increase anomalous near-surface convergence in the tropical western Pacific, which fuels anomalous upward vertical motions (dot over the cloud symbols in Fig. 17b) that, in turn, sustain preexisting anomalous convection. This leads to anomalous divergence aloft (red shaded oval

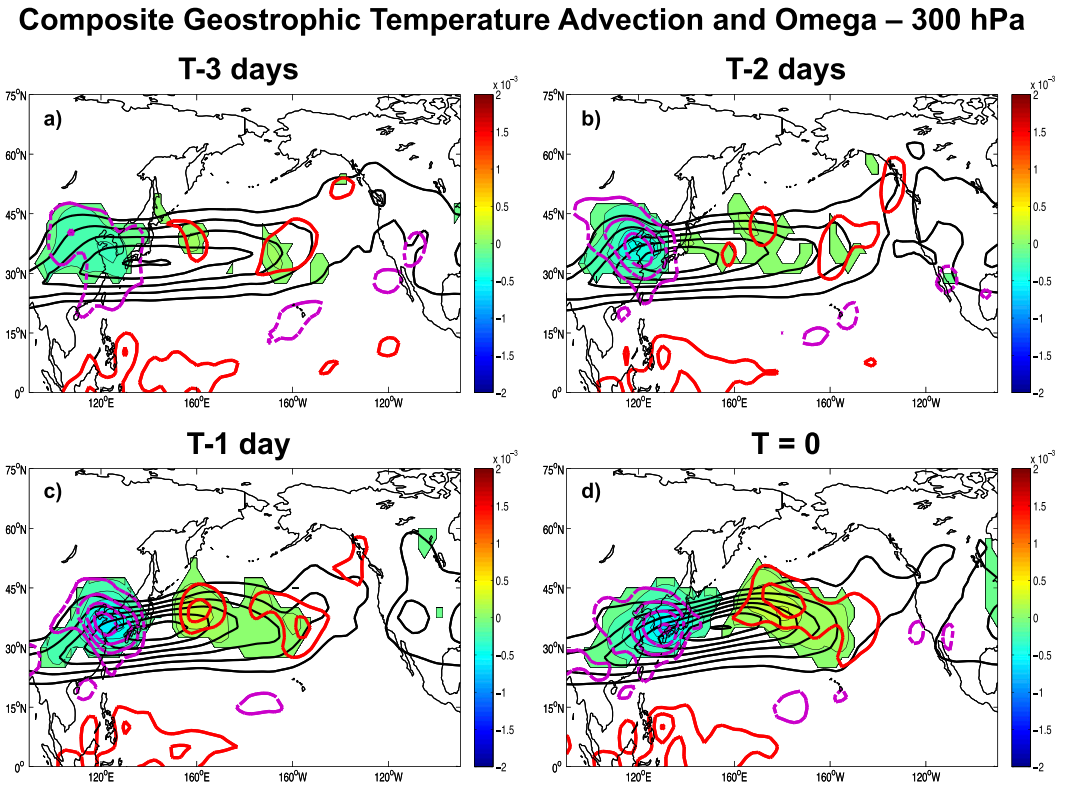

FIG. 16. The 300-hPa composite geostrophic temperature advection (fill pattern; K s^{-1}) and vertical motion [red (purple) solid (dashed) contour indicates upward (downward) vertical motion] contoured every 0.05 Pa s^{-1} starting at ±0.05 Pa s^{-1} for times (a) 3 days prior to jet superposition, (b) 2 days prior to jet superposition, (c) 1 day prior to jet superposition, and (d) at time of jet superposition. Also plotted on all panels is the 300-hPa composite wind speed (black solid contour) every 10 m s^{-1} starting at 30 m s^{-1}.

with black dot in center in Fig. 17b). An attendant region of anomalous convergence aloft poleward and above the region of cold air is also present, associated with anomalous subsidence via mass continuity (blue circle with cross in Fig. 17b).

High-θ_e, low-PV convective outflow on the equatorward side of the jet is advected by the anomalous anticyclonic flow east of the anomalous convection (brown arrows with the letter H in Fig. 17c). Given that this air has $\theta_e \approx 350$ K, as it is advected poleward, it is locally exhausted within the STJ isentropic layer on the equatorward side of the composite jet (jet symbol with black contour in Fig. 17c). The movement of this air into the STJ layer on the anticyclonic shear side of the jet increases the anomalous pressure depth. This not only induces anomalous anticyclonic shear equatorward of the jet, enhancing the anomalous wind speed within the jet core, but also acts to reduce the PV on the equatorward side of the jet core such that the PV gradient (i.e., in the 1–3-PVU channel) associated with the jet becomes stronger and more vertically oriented (Fig. 17d).

On the cyclonic shear side of the composite jet, geostrophic cold air advection in cyclonic shear drives subsidence through the jet core in its entrance region, transporting high-PV air downward and thus increasing the strength of the positive PV anomaly poleward of the jet core (Figs. 15, 16). This positive PV anomaly plays a role in increasing the magnitude of the 1–3-PVU gradient as well as in shaping the PV wall into a more vertical orientation. The increase in anomalous wind speed coincident with the development of a deep and vertical PV wall are the hallmarks of a western Pacific vertical jet superposition.

This conceptual model shows many elements of the various conceptual models and results from Chang et al. (1979), Chang and Lau (1980), and Wu and Chan (1997). For example, as shown in Fig. 14 of Chang and Lau (1980), as cold air on the eastern side of the Siberian–Mongolian high (SMH) is advected equatorward, the associated strong northerly winds may lead to enhanced surface convergence in the western Pacific equatorial region. This convergence sustains preexisting tropical convection in the equatorial western Pacific, which, in turn, enhances the local Hadley cell circulation (Chang and Lau 1980; Wu and Chan 1997). Enhanced poleward flow associated with the invigorated Hadley cell

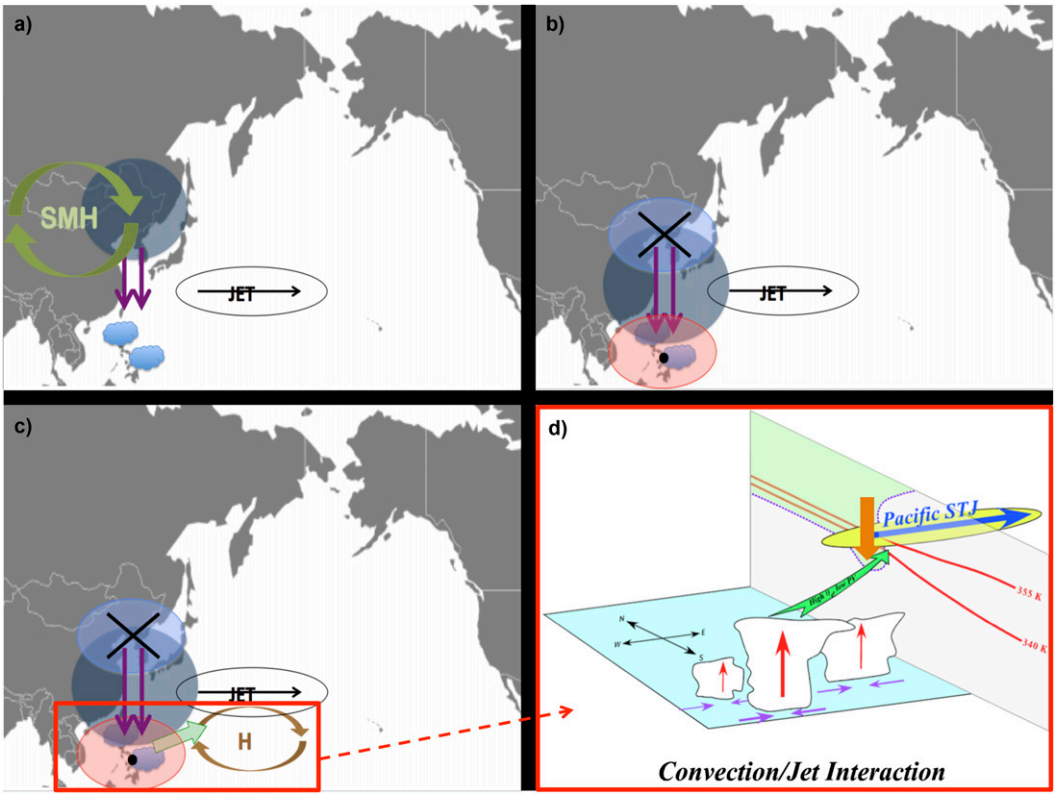

FIG. 17. Conceptual model outlining the role of tropical forcing with respect to onset of robust vertical jet superposition events in the western Pacific. (a) The green arrows represent the Siberian–Mongolian high; the purple arrows represent near-surface anomalous northerly winds; the blue cloud symbols represent anomalous tropical convection; and the black thin circle with the westerly vector represents the approximate position of the composite jet. All features in (a) are present 3 days prior to composite vertical jet superposition. (b) The blue (red) circle indicates the region of anomalous upper-tropospheric convergence (divergence), with the cross (dot) symbol representing anomalous downward (upward) vertical motion within the air column. (c) The brown arrows with the letter H in the center represent the anomalous geopotential height maximum feature on the antiyclonic shear side of the jet that develops 48 h prior to composite jet superposition. The hatched green arrow represents the direction of transport of high-θ_e, low-PV air mass from the tropics toward the region where the anomalous anticyclone develops equatorward of the jet. (d) The role of low-PV, high-θ_e air associated with tropical convective outflow as it is transported into the STJ isentropic layer equatorward of the superposed jet. The orange arrow represents subsidence within the jet entrance region that plays a role in the development of the deep, vertical PV wall associated with the composite superposed jet. See text for further explanation.

induces a stronger western Pacific jet via enhanced angular momentum transport.

In Chang et al. (1979) and Chang and Lau (1980), it was shown that EAWM cold surge events induce enhanced surface convergence in the western Pacific equatorial region, which helps to intensify the local Hadley cell circulation in the region and subsequently enhance the speed of the western Pacific jet. While the present analysis shows an enhancement of the jet in this region associated with the presence of a cold surge, it appears in our conceptual model as a component of the larger-scale evolution of an environment that produces a vertical superposition of the usually separate polar and subtropical jets. Those physical mechanisms associated with EAWM cold surges that strengthen the western Pacific jet appear to be vital elements in the development of western Pacific superposition events.

It is interesting to note that, even within the climatological cross section through the jet core (Fig. 7a), only two steps in the tropopause are evident, implying that the western Pacific jet borders on a superposed structure rather frequently, as suggested by Christenson (2013). The foregoing analysis, however, makes clear that, despite the temptation to consider the western Pacific jet as a single monolithic feature, only the correct collection of circumstances can foster production of the relatively rare vertical jet superposition. It appears that cold surge events, associated as they are with an increase in the

strength of the western Pacific jet entrance region circulation, the transport of high-θ_e, low-PV air into the STJ isentropic layer, and the occurrence of geostrophic cold air advection in cyclonic shear in the jet entrance region, are key physical mechanisms that help to induce robust vertical jet superposition.

A number of additional research questions remain to be explored in the wake of the foregoing analysis. For example, although several of the air parcel trajectories in Fig. 14 trace back to the region of negative anomalous OLR near Indonesia, further trajectory analysis is required to investigate the percentage of cases in which the low-PV, high-θ_e air on the equatorward flank of the superposed jet core is transported upward directly from the tropical boundary layer.

The cold surges in our composite results play a key role in producing jet superpositions. Therefore, understanding the mechanisms triggering these cold surge events would further illuminate our conception of the life cycle of western Pacific jet superpositions. For example, it has been shown that cold surges in East Asia can result from the propagation of a Rossby wave train from central Eurasia southeastward, noted as a wave train of "Atlantic origin" (Takaya and Nakamura 2005). We suggest that repeating our composite analysis for days prior to $T - 3$ would lend additional insight into the development of cold surges.

It would also be beneficial to investigate the downstream effects of western Pacific jet superpositions on weather events throughout the Northern Hemisphere. This topic can be investigated using the same composite analysis technique we use in our methodology, investigating times up to several days after composite jet superposition (i.e., composite analysis at times $T + 1, T + 2, \ldots, T + 5$ days). Such an analysis would provide further understanding of any relationship that these events have with other large-scale Northern Hemisphere teleconnections and thus support improved understanding and prediction of significant weather events that derive from western Pacific jet superpositions. Finally, given the significant correlation between various EAWM indices and the number of jet superposition IDs in our western Pacific interest region, it is of interest to compare and contrast the physical processes leading to jet superposition within strong versus weak EAWM seasons. Such analyses are currently ongoing.

Acknowledgments. We thank the two anonymous reviewers for their constructive feedback. We also thank Rich Pawlowicz for making the M_Map MATLAB mapping package available for public use for plotting high-resolution continental borders. NCEP–NCAR Reanalysis 1 and OLR data were obtained from the NOAA/OAR/ESRL PSD, Boulder, Colorado, from http://www.esrl.noaa.gov/psd/. This work is funded by the National Science Foundation through Grant AGS-1265182.

REFERENCES

Bosart, L. F., G. J. Hakim, K. R. Tyle, M. A. Bedrick, W. E. Bracken, M. J. Dickinson, and D. M. Schultz, 1996: Large-scale antecedent conditions associated with the 12–14 March 1993 cyclone ("Superstorm '93") over eastern North America. *Mon. Wea. Rev.*, **124**, 1865–1891, doi:10.1175/1520-0493(1996)124<1865:LSACAW>2.0.CO;2.

Boyle, J. S., and T.-J. Chen, 1987: Synoptic aspects of the wintertime East Asian monsoon. *Monsoon Meteorology*, C.-P. Chang and T. N. Krishnamurti, Eds., Oxford University Press, 125–160.

Chan, J. C. L., and C. Y. Li, 2004: The East Asian winter monsoon. *The Asian Monsoon*, C. Chang, Ed., World Scientific, 54–106.

Chang, C.-P., and K.-M. Lau, 1980: Northeasterly cold surges and near-equatorial disturbances over the winter MONEX area during December 1974. Part II: Planetary-scale aspects. *Mon. Wea. Rev.*, **108**, 298–312, doi:10.1175/1520-0493(1980)108<0298:NCSANE>2.0.CO;2.

——, J. Erickson, and K.-M. Lau, 1979: Northeasterly cold surges and near-equatorial disturbances over the winter MONEX area during December 1974. Part I: Synoptic aspects. *Mon. Wea. Rev.*, **107**, 812–829, doi:10.1175/1520-0493(1979)107<0812:NCSANE>2.0.CO;2.

Chin, P., 1969: Cold surges over South China. Royal Observatory, Hong Kong, Tech. Note 28, 40 pp.

Christenson, C. E., 2013: A synoptic-climatology of Northern Hemisphere polar and subtropical jet superposition events. M.S. thesis, Dept. of Atmospheric and Oceanic Sciences, University of Wisconsin–Madison, 62 pp.

Cunningham, P., and D. Keyser, 2004: Dynamics of jet streaks in a stratified quasi-geostrophic atmosphere: Steady-state representations. *Quart. J. Roy. Meteor. Soc.*, **130**, 1579–1609, doi:10.1256/qj.03.35.

Defant, F., and H. Taba, 1957: The threefold structure of the atmosphere and the characteristics of the tropopause. *Tellus*, **9**, 259–275, doi:10.1111/j.2153-3490.1957.tb01884.x.

Draxler, R. R., 1999: HYSPLIT_4 user's guide. NOAA Tech. Memo. ERL ARL-230, 51 pp.

——, and G. D. Hess, 1997: Description of the HYSPLIT_4 modeling system. NOAA Tech. Memo. ERL ARL-224, 24 pp.

——, and ——, 1998: An overview of the HYSPLIT_4 modelling system of trajectories, dispersion, and deposition. *Aust. Meteor. Mag.*, **47**, 295–308.

——, and G. D. Rolph, 2015: HYSPLIT–Hybrid Single Particle Lagrangian Integrated Trajectory Model. NOAA Air Resources Laboratory, accessed 4 December 2015. [Available online at http://ready.arl.noaa.gov/HYSPLIT.php.]

Eliassen, A., 1962: On the vertical circulation in frontal zones. *Geophys. Publ.*, **24**, 147–160.

Hakim, G. J., D. Keyser, and L. F. Bosart, 1996: The Ohio valley wave-merger cyclogenesis event of 25–26 January 1978. Part II: Diagnosis using quasigeostrophic potential vorticity inversion. *Mon. Wea. Rev.*, **124**, 2176–2205, doi:10.1175/1520-0493(1996)124<2176:TOVWMC>2.0.CO;2.

Hoskins, B. J., and P. Berrisford, 1988: A potential vorticity perspective of the storm of 15–16 October 1987. *Weather*, **43**, 122–129, doi:10.1002/j.1477-8696.1988.tb03890.x.

Jhun, J. G., and E. J. Lee, 2004: A new East Asian winter monsoon index and associated characteristics of the winter monsoon. *J. Climate*, **17**, 711–726, doi:10.1175/1520-0442(2004)017<0711:ANEAWM>2.0.CO;2.

Kalnay, E., and Coauthors, 1996: The NCEP/NCAR 40-Year Reanalysis Project. *Bull. Amer. Meteor. Soc.*, **77**, 437–471, doi:10.1175/1520-0477(1996)077<0437:TNYRP>2.0.CO;2.

Keyser, D., and M. J. Pecnick, 1985: A two-dimensional primitive equation model of frontogenesis forced by confluence and horizontal shear. *J. Atmos. Sci.*, **42**, 1259–1282, doi:10.1175/1520-0469(1985)042<1259:ATDPEM>2.0.CO;2.

——, and M. A. Shapiro, 1986: A review of the structure and dynamics of upper-level frontal zones. *Mon. Wea. Rev.*, **114**, 452–499, doi:10.1175/1520-0493(1986)114<0452:AROTSA>2.0.CO;2.

Koetswaram, P., 1953: An analysis of the high tropospheric wind circulation over India in winter. *Indian J. Meteor. Geophys.*, **4**, 13–21.

——, and S. Parthasarathy, 1954: The mean jet stream over India in the pre-monsoon and post-monsoon seasons and vertical motions associated with subtropical jet streams. *Indian J. Meteor. Geophys.*, **5**, 138–156.

Krishnamurti, T. N., 1961: On the role of the subtropical jet stream of winter in the atmospheric general circulation. *J. Meteor.*, **18**, 657–670, doi:10.1175/1520-0469(1961)018<0657:OTROTS>2.0.CO;2.

Lee, Y.-Y., G.-H. Lim, and J.-S. Kug, 2010: Influence of the East Asian winter monsoon on the storm track activity over the North Pacific. *J. Geophys. Res.*, **115**, D09102, doi:10.1029/2009JD012813.

Loewe, F., and V. Radok, 1950a: A meridional aerological cross section in the southwest Pacific. *J. Meteor.*, **7**, 58–65, doi:10.1175/1520-0469(1950)007<0058:AMACSI>2.0.CO;2.

——, and ——, 1950b: Some amendments to ''A meridional aerological cross section in the southwest Pacific.'' *J. Meteor.*, **7**, 305–306, doi:10.1175/1520-0469(1950)007<0306:SATAMA>2.0.CO;2.

Martin, J. E., 2014: Quasi-geostrophic diagnosis of the influence of vorticity advection on the development of upper level jet-front systems. *Quart. J. Roy. Meteor. Soc.*, **140**, 2658–2671, doi:10.1002/qj.2333.

Mohri, K., 1953: On the fields of wind and temperature over Japan and adjacent waters during winter of 1950–1951. *Tellus*, **5A**, 340–358, doi:10.1111/j.2153-3490.1953.tb01066.x.

Morrice, A. M., 1973: Quantitative forecasting of the winter monsoon in Hong Kong. Royal Observatory, Hong Kong, Tech. Note 35, 41 pp.

Namias, J., and P. F. Clapp, 1949: Confluence theory of the high tropospheric jet stream. *J. Meteor.*, **6**, 330–336, doi:10.1175/1520-0469(1949)006<0330:CTOTHT>2.0.CO;2.

Newton, C. W., 1954: Frontogenesis and frontolysis as a three-dimensional process. *J. Meteor.*, **11**, 449–461, doi:10.1175/1520-0469(1954)011<0449:FAFAAT>2.0.CO;2.

Palmén, E., and C. W. Newton, 1969: *Atmospheric Circulation Systems: Their Structure and Physical Interpretation.* Academic Press, 603 pp.

Reiter, E. R., 1961: *Meteorologie der Strahlströme (Meteorology of the Jet Streams).* Springer-Verlag, 473 pp.

——, 1963: *Jet Stream Meteorology.* University of Chicago Press, 515 pp.

——, and L. F. Whitney, 1969: Interaction between subtropical and polar-front jet stream. *Mon. Wea. Rev.*, **97**, 432–438, doi:10.1175/1520-0493(1969)097<0432:IBSAPJ>2.3.CO;2.

Riehl, H., 1962: Jet streams of the atmosphere. Dept. of Atmospheric Science, Colorado State University Tech. Rep. 32, 117 pp.

Rolph, G. D., 2015: READY–Real-Time Environmental Applications and Display System. NOAA Air Resources Laboratory, accessed 4 December 2015. [Available online at http://ready.arl.noaa.gov.]

Shapiro, M. A., 1982: Mesoscale weather systems of the central United States. CIRES Tech. Rep., 78 pp.

——, and D. Keyser, 1990: Fronts, jet streams, and the tropopause. *Extratropical Cyclones: The Erik Palmén Memorial Volume*, C. Newton and E. O. Holopainen, Eds., Amer. Meteor. Soc., 167–191.

Sutcliffe, R. C., and J. K. Bannon, 1954: Seasonal changes in the upper-air conditions in the Mediterranean–Middle East area. *Scientific Proc., IUGG Association of Meteorology*, Rome, Italy, Int. Union of Geodesy and Geophysics, 322–334.

Takaya, K., and H. Nakamura, 2005: Geographical dependence of upper-level blocking formation associated with intraseasonal amplification of the Siberian high. *J. Atmos. Sci.*, **62**, 4441–4449, doi:10.1175/JAS3628.1.

Wang, L., and W. Chen, 2010: How well do existing indices measure the strength of the East Asian winter monsoon? *Adv. Atmos. Sci.*, **27**, 855–870, doi:10.1007/s00376-009-9094-3.

——, and ——, 2014: An intensity index for the East Asian winter monsoon. *J. Climate*, **27**, 2361–2374, doi:10.1175/JCLI-D-13-00086.1.

——, ——, W. Zhou, and R. Huang, 2009: Interannual variations of East Asian trough axis at 500 hPa and its association with the East Asian winter monsoon pathway. *J. Climate*, **22**, 600–614, doi:10.1175/2008JCLI2295.1.

Winters, A. C., and J. E. Martin, 2014: The role of a polar/subtropical jet superposition in the May 2010 Nashville flood. *Wea. Forecasting*, **29**, 954–974, doi:10.1175/WAF-D-13-00124.1.

Wu, M. C., and J. C. L. Chan, 1997: Upper-level features associated with winter monsoon surges over south China. *Mon. Wea. Rev.*, **125**, 317–340, doi:10.1175/1520-0493(1997)125<0317:ULFAWW>2.0.CO;2.

Yang, S., K. M. Lau, and K. M. Kim, 2002: Variations of the East Asian jet stream and Asian–Pacific–American winter climate anomalies. *J. Climate*, **15**, 306–325, doi:10.1175/1520-0442(2002)015<0306:VOTEAJ>2.0.CO;2.

Yeh, T. C., 1950: The circulation of the high troposphere over China in the winter of 1945–46. *Tellus*, **2A**, 173–183, doi:10.1111/j.2153-3490.1950.tb00329.x.

Yen, M.-C., and T.-C. Chen, 2002: A revisit of the tropical–midlatitude interaction in East Asia caused by cold surges. *J. Meteor. Soc. Japan*, **80**, 1115–1128, doi:10.2151/jmsj.80.1115.